26. Bode C, Bode JC. Activation of the innate immune system and alcoholic liver disease: effects of ethanol per se or enhanced intestinal translocation of bacterial toxins induced by ethanol? Alcohol Clin Exp Res 2005;29:166S-171S.

27. Tsukamoto H. Redox regulation of cytokine expression in Kupffer cells. Antioxid Redox Signal 2002;4:741-748.

28. Brock RW, Lawlor DK, Harris KA, Potter RF. Initiation of remote hepatic injury in the rat: interactions between Kupffer cells, tumor necrosis factor-alpha, and microvascular perfusion. Hepatology 1999;30:137-142.

29. Gao B. Hepatoprotective and anti-inflammatory cytokines in alcoholic liver disease. J Gastroenterol Hepatol 2012;27 Suppl 2:89-93.

30. Zhao XJ, Dong Q, Bindas J, Piganelli JD, Magill A, Reiser J, Kolls JK. TRIF and IRF-3 binding to the TNF promoter results in macrophage TNF dysregulation and steatosis induced by chronic ethanol. J Immunol 2008;181:3049-3056.

FIGURE LEGENDS

Figure 1. ***Alcohol feeding increases hepatic, plasma, biliary and fecal OPN levels.*** WT, *Opn*$^{-/-}$ and *Opn*^{HEP} Tg mice were fed 7 wks either the control or the alcohol Lieber-DeCarli diet. qRT-PCR analysis of liver *Opn* mRNA **(A)**. Computer-assisted morphometric analysis of the OPN IHC **(B)**. There is increased OPN expression in *Opn*^{HEP} Tg compared to WT mice with additional enhancement by ethanol feeding (green arrows) as shown on IHC. PV: portal vein. CV: central vein. BD: bile duct **(C)**. Plasma **(D)**, bile **(E)** and fecal **(F)** OPN levels. *n*=10/group; **p*<0.05 and ***p*<0.01 for ethanol *vs* control; •*p*<0.05, ••*p*<0.01 and •••*p*<0.001 for *Opn*^{HEP} Tg *vs* WT mice.

Figure 2. ***Natural induction plus overexpression of OPN in hepatocytes protects from early alcohol-induced liver injury whereas natural induction of OPN does not suffice to confer full protection.*** WT, *Opn*$^{-/-}$ and *Opn*^{HEP} Tg mice were fed 7 wks either the control or the alcohol Lieber-DeCarli diet. Liver-to-body weight ratio **(A)**, serum ALT activity **(B)**, serum LPS levels **(C**, left**)** and liver bacterial *16S* rRNA **(C**, right**)**. Serum ethanol concentration **(D)**. Serum and liver TG **(E)** and LDL plus VLDL **(F)**. *n*=10/group; **p*<0.05 and ***p*<0.01 for ethanol *vs* control; •*p*<0.05 and ••*p*<0.01 for any genotype *vs* WT mice.

Figure 3. ***Natural induction plus overexpression of OPN in hepatocytes protects from alcohol-induced steatosis whereas natural induction of OPN does not suffice to confer full protection.*** WT, *Opn*$^{-/-}$ and *Opn*^{HEP} Tg mice were fed 7 wks either the control or the alcohol Lieber-DeCarli diet. H&E staining shows less inflammation, hepatocyte ballooning degeneration (red arrows on the insets), micro- (yellow arrows) and macrovesicular (green arrows) steatosis in ethanol-treated *Opn*^{HEP} Tg followed by WT and by *Opn*$^{-/-}$ mice. PV: portal vein. CV: central

vein **(A)**. The scores for inflammation **(B)**, hepatocyte ballooning degeneration **(C)** and steatosis **(D)** are lower in ethanol-treated *Opn*^{HEP} Tg followed by WT and *Opn*$^{-/-}$ mice. Morphometric analysis **(E)** and oil red O staining **(F)**. *n*=10/group; **p*<0.05 for ethanol *vs* control; •*p*<0.05 and ••*p*<0.01 for any genotype *vs* WT mice.

Figure 4. ***TNFα expression remains basal in ethanol-fed*** **Opn**^{HEP} ***Tg but increases in ethanol-fed WT and more in Opn***$^{-/-}$ ***mice.*** WT, *Opn*$^{-/-}$ and *Opn*^{HEP} Tg mice were fed 7 wks either the control or the alcohol Lieber-DeCarli diet. TNFα IHC depicts a small number of TNFα^{+} cells (red arrows) in ethanol-treated *Opn*^{HEP} Tg compared to WT and *Opn*$^{-/-}$ mice **(A)**. Computer-assisted morphometric analysis of the TNFα IHC calculated as the number of TNFα^{+} cells in 20 fields at 200x magnification **(B**, left**)**. Western blot analysis for liver membrane-bound and soluble along with plasma TNFα protein **(B**, right**)**. IHC for F4/80 (red arrows) **(C)** and morphometric analysis of the F4/80 IHC calculated as the number of F4/80^{+} cells in 20 fields at 200x magnification **(D)**. Co-localization of TNFα^{+} and F4/80^{+} staining in ethanol-fed WT mice (merged=yellow) **(E)**. Co-localization of OPN^{+} and F4/80^{+} staining in ethanol-fed WT, *Opn*$^{-/-}$ and *Opn*^{HEP} Tg mice (merged=yellow) **(F)**. *n*=10/group; **p*<0.05, ***p*<0.01 and ****p*<0.001 for ethanol *vs* control; •*p*<0.05 and ••*p*<0.01 for any genotype *vs* WT mice.

Figure 5. ***OPN binds LPS and prevents macrophage activation, ROS plus RNS generation and lowers TNFα expression.*** The ability of human biotinylated m-OPN* to bind LPS is demonstrated on LPS-coated plates. Incubation with an excess of BSA does not out-compete the m-OPN* binding whereas incubation with non-biotinylated human m-OPN outcompetes the m-OPN* binding to LPS (AU: absorbance units). ***p*<0.01 *vs* control and ••*p*<0.01 for competition studies *vs* biotinylated m-OPN **(A**, top**)**. Using surface plasmon resonance, the lipid A moiety of LPS was immobilized onto a hydrophobic surface and the monolayer was incubated

with increasing concentrations of rOPN, LBP, m-OPN or BSA. Sensograms showing that all molecules bind lipid A but differ in their binding affinity **(A**, bottom**)**. Flow cytometry analysis of the binding of FITC-LPS to RAW 264.7 macrophages incubated in the presence or absence of rOPN **(B**, left; ***a:*** control, ***b:*** FITC-LPS and ***c:*** FITC-LPS + rOPN**)** along with TLR4 and MD2 neutralizing Abs **(B**, right**)**. The generation of intra- and extracellular hydroperoxides **(C)** along with extracellular nitrates plus nitrites **(D)** by stimulation of RAW 264.7 macrophages with LPS is partially blocked by co-treatment with rOPN. *Tnfα* mRNA **(E)** along with intra- and extracellular TNFα protein **(F**, top**)** increase under LPS treatment but decrease time-dependently by co-incubation of RAW 264.7 macrophages with rOPN. Levels of TNFα in human Kupffer cells **(F**, bottom**)**. n=10; ***p<0.001 for LPS-treated *vs* its own control; •p<0.05, ••p<0.01 and •••p<0.001 for rOPN co-treated *vs* its own control.

Figure 6. ***m-OPN prevents FITC-LPS translocation*** **in vivo** ***in*** **Opn$^{-/-}$** ***mice.*** To measure intestinal permeability, an ileal loop model using *Opn*$^{-/-}$ mice was performed. A 4-cm long segment of the mouse ileum was created using two vascular hemoclips without disrupting the mesenteric vascular arcades and under anesthesia. The portion of intestine between the two clips was injected with FITC-LPS in addition to m-OPN or BSA (control) and mice were sacrificed. FITC-LPS^{+} staining is present in the ileal loop villi from FITC-LPS + BSA injected mice but is almost absent in FITC-LPS + m-OPN injected mice **(A)**. Morphometric analysis of the FITC-LPS positive area **(B)**. Plasma FITC-LPS is shown in **(C)**. n=6; •p<0.05 for FITC-LPS + m-OPN *vs* FITC-LPS + BSA.

Figure 7. ***Treatment with m-OPN rescues WT mice from alcohol-induced liver injury.*** WT mice were fed either the control or the ethanol Lieber-DeCarli diet for 3 wks following which mice were given ethanol in combination with 200 µg/ml BSA or with m-OPN for 10 days. H&E

staining shows micro- (yellow arrows) and macrovesicular (green arrows) steatosis by ethanol feeding plus BSA, which is partially prevented by treatment with m-OPN. PV: portal vein. CV: central vein **(A)**. The scores for inflammation, hepatocyte ballooning degeneration and steatosis **(B)**. Serum ALT activity **(C)** and LPS levels **(D)**. *n*=6; •p<0.05 and ••p<0.01 for m-OPN *vs* BSA. ***Proposed mechanism:*** overexpression of OPN in hepatocytes under alcohol consumption contributes to enhance its secretion into the plasma and/or its excretion into the bile and feces to reach sufficient levels. The presence of OPN in feces blunts the increase in LPS translocation. This is also validated by oral treatment with m-OPN. Likewise, binding of OPN to LPS prevents macrophage infiltration and activation blocking the increase in TNFα, ROS and RNS; hence, lowering alcohol-induced liver injury and steatosis **(E)**.

OTHER MANUSCRIPT ELEMENTS

Acknowledgment

The authors are very grateful to Drs. David T. Denhardt (Rutgers University, NJ) for his generous gift of the 2A1 Ab, Kang Chen (Mount Sinai School of Medicine, NY) for his assistance with the flow cytometry assays and Ning Wang (Department of Central Laboratory, Southwest Hospital, China) for her assistance in the binding experiments using the IAsys Plus System. We are also very thankful to all past and current members from the Nieto Laboratory for their helpful comments and suggestions throughout the course of this project.

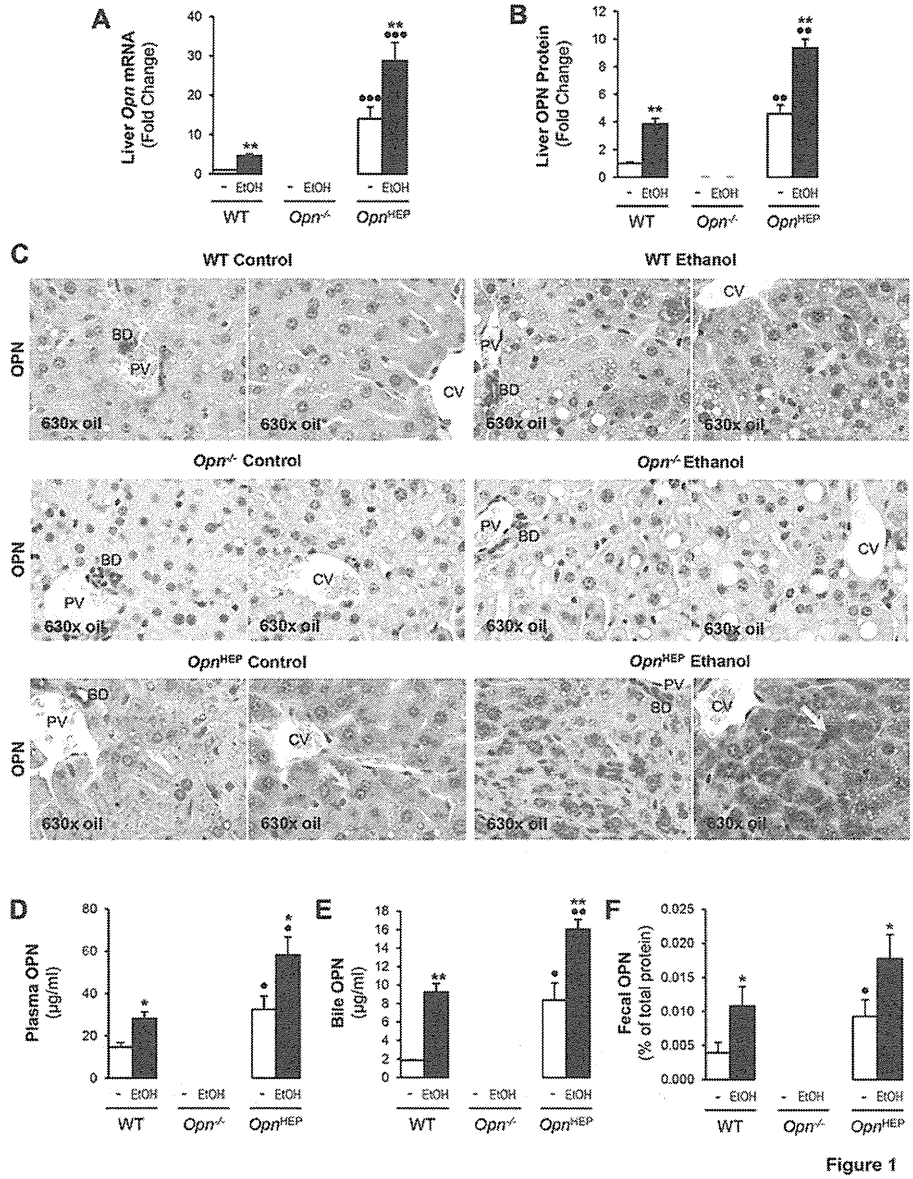

Figure 1

76x96mm (300 x 300 DPI)

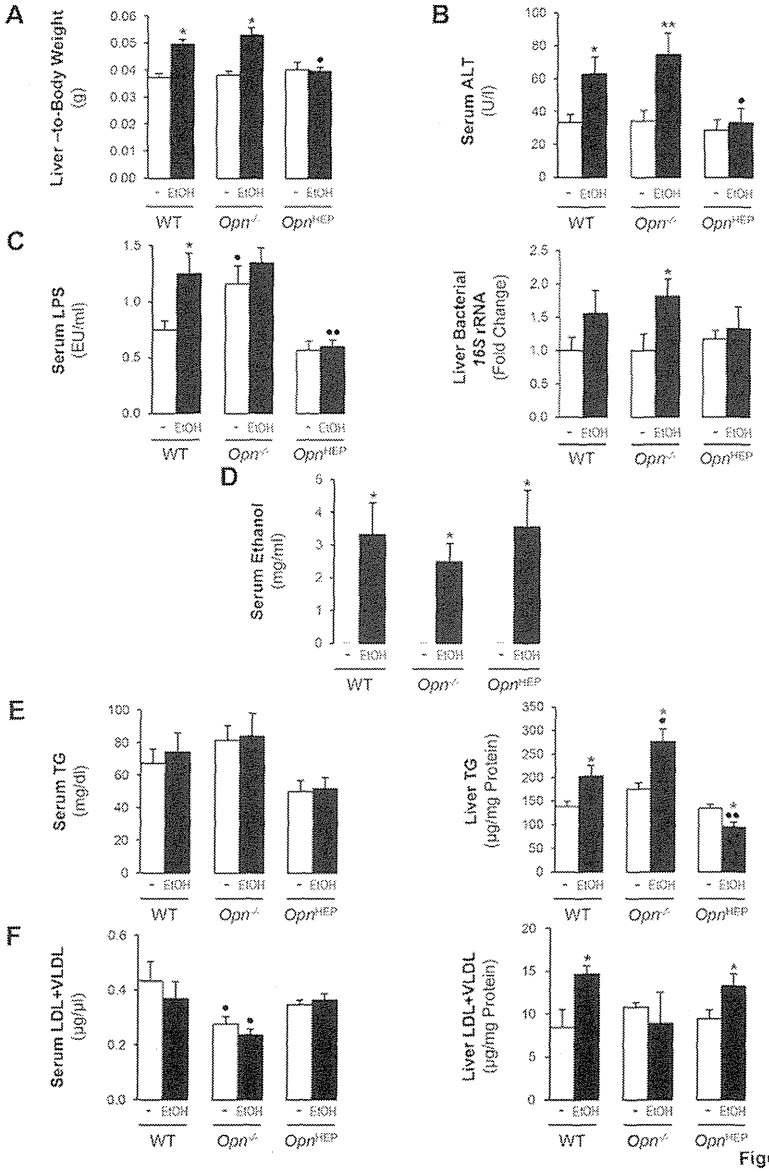

Figure 2

76x99mm (300 x 300 DPI)

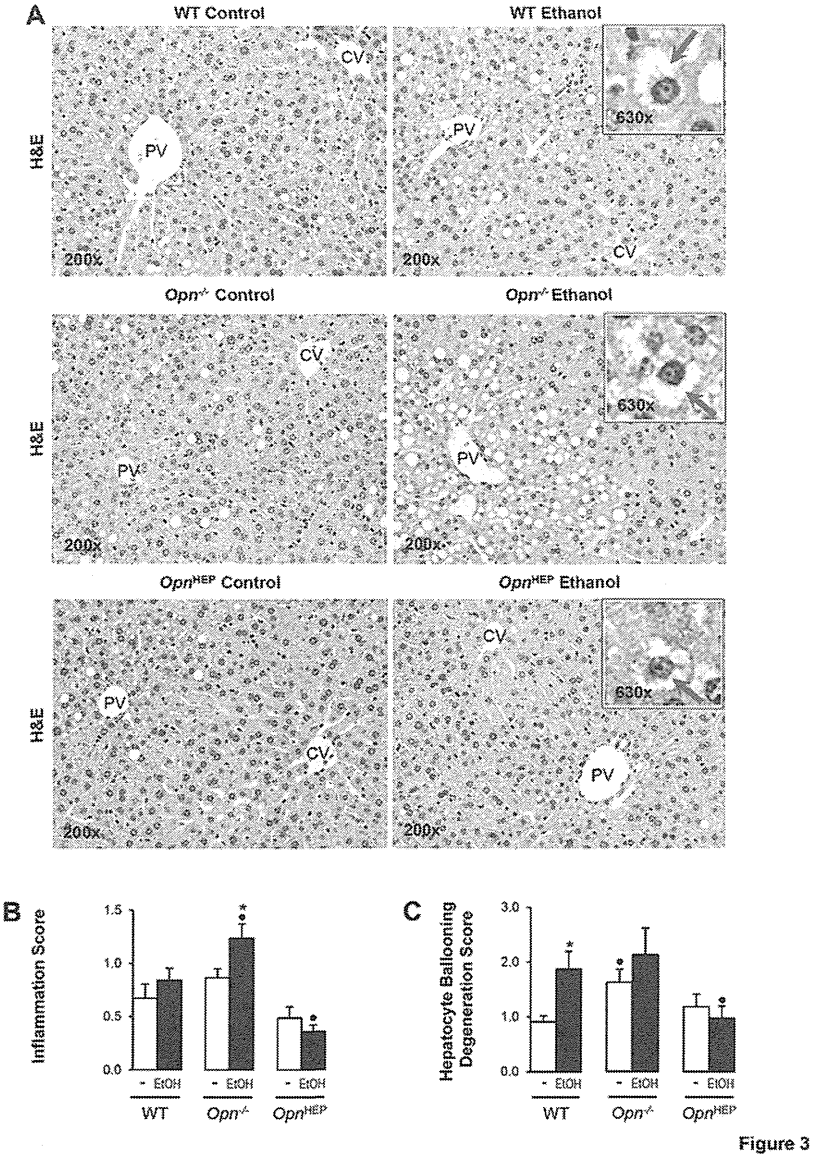

Figure 3

76x99mm (300 x 300 DPI)

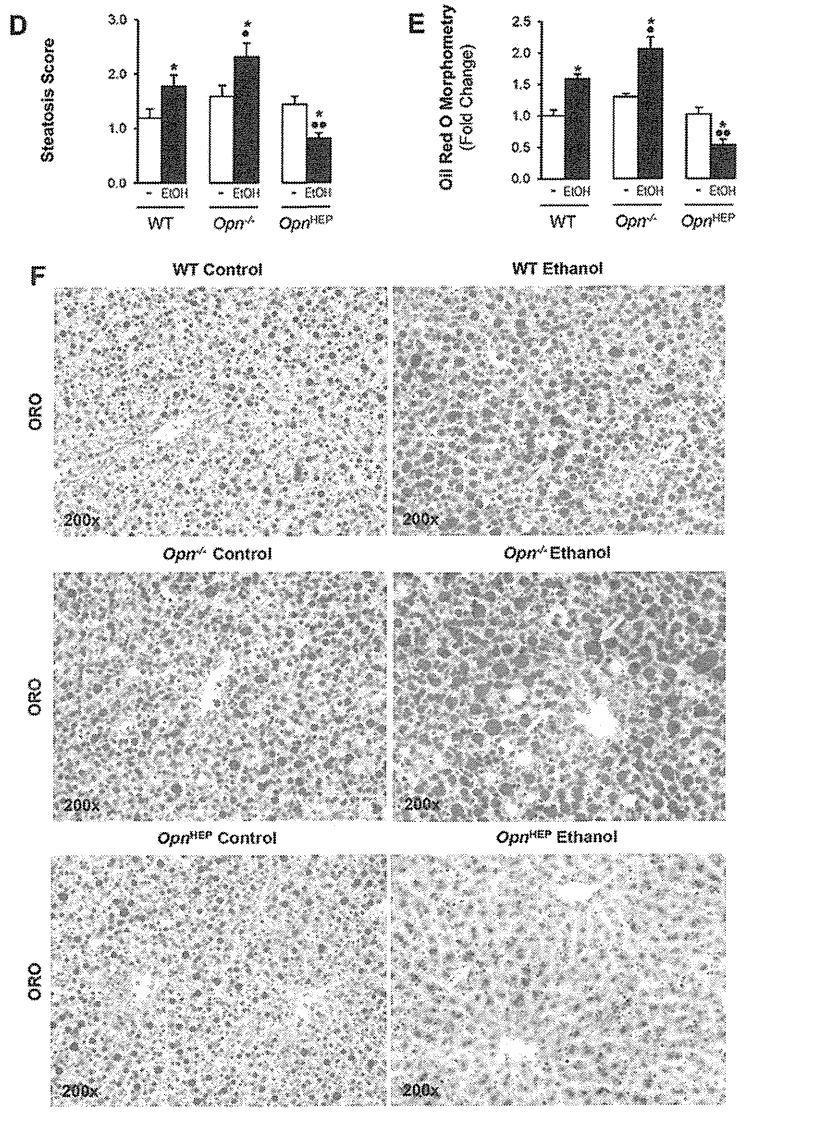

Figure 3 Continuation

76x99mm (300 x 300 DPI)

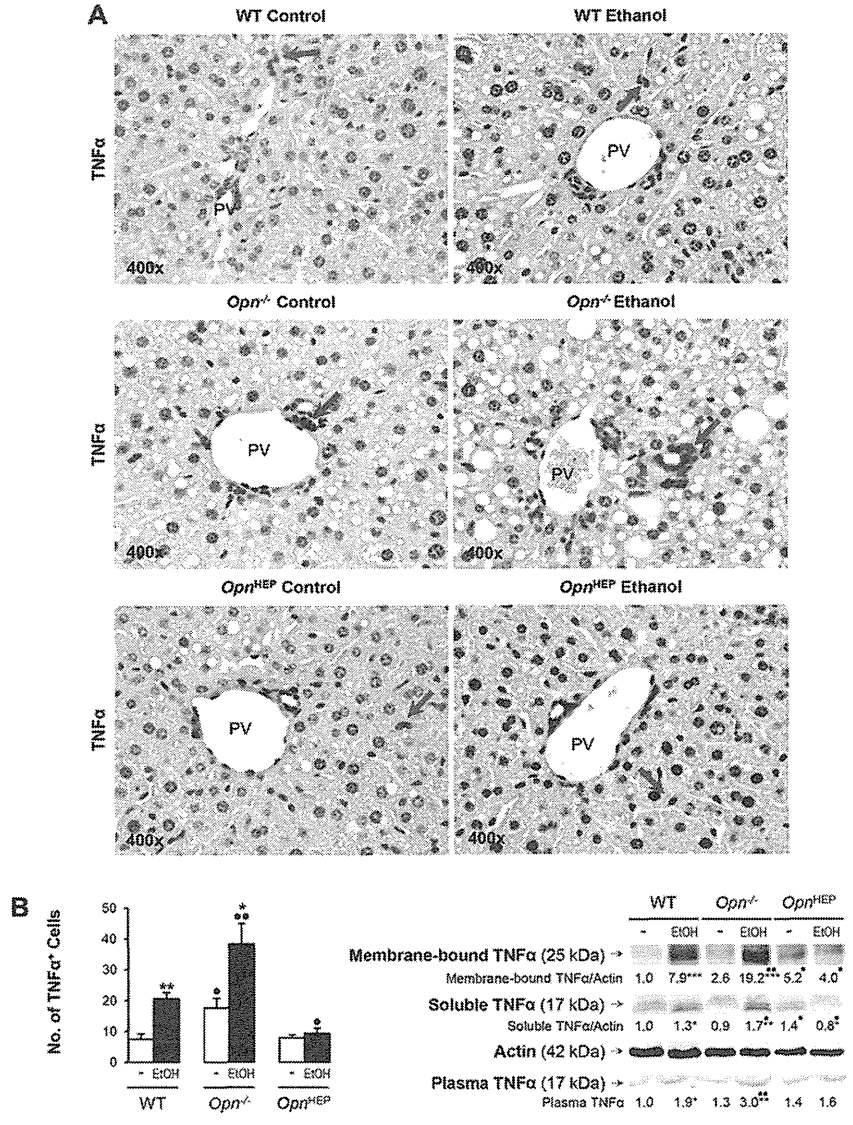

Figure 4

76x99mm (300 x 300 DPI)

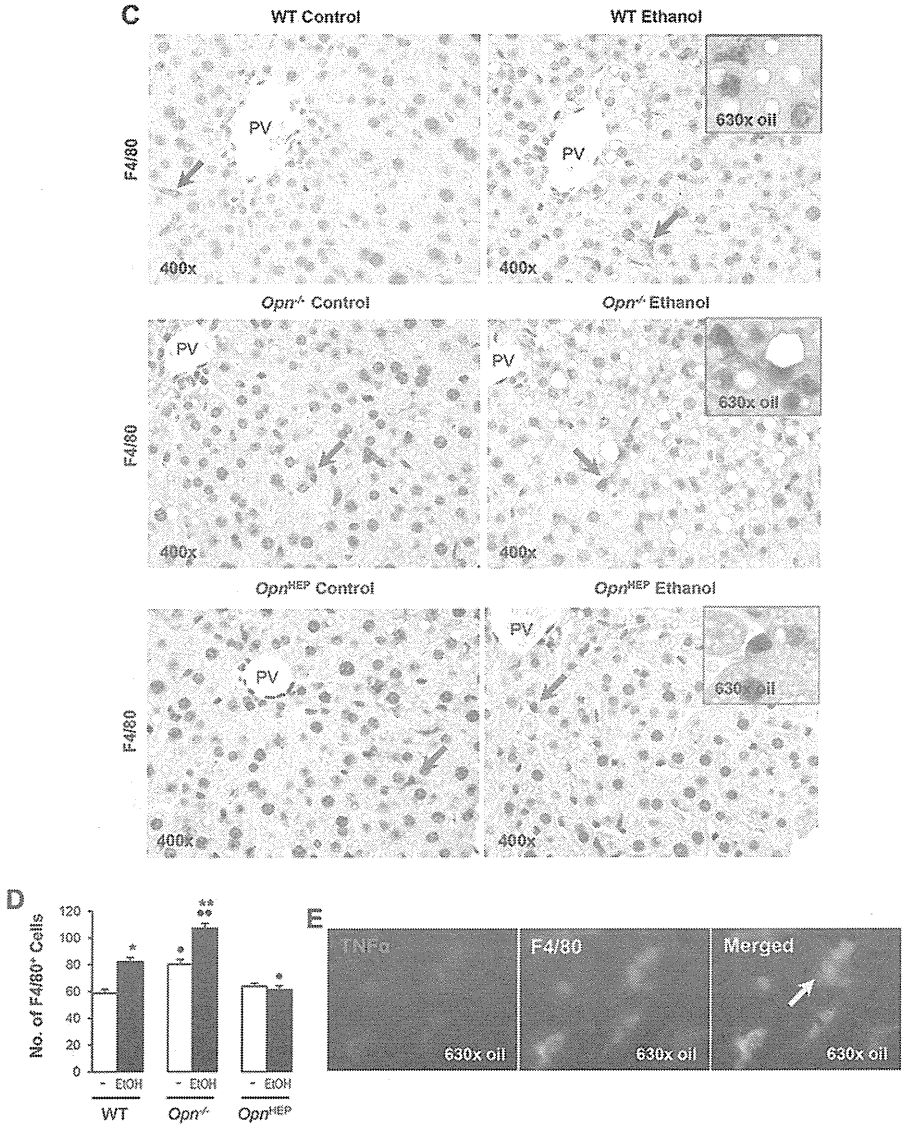

Figure 4 Continuation

76x96mm (300 x 300 DPI)

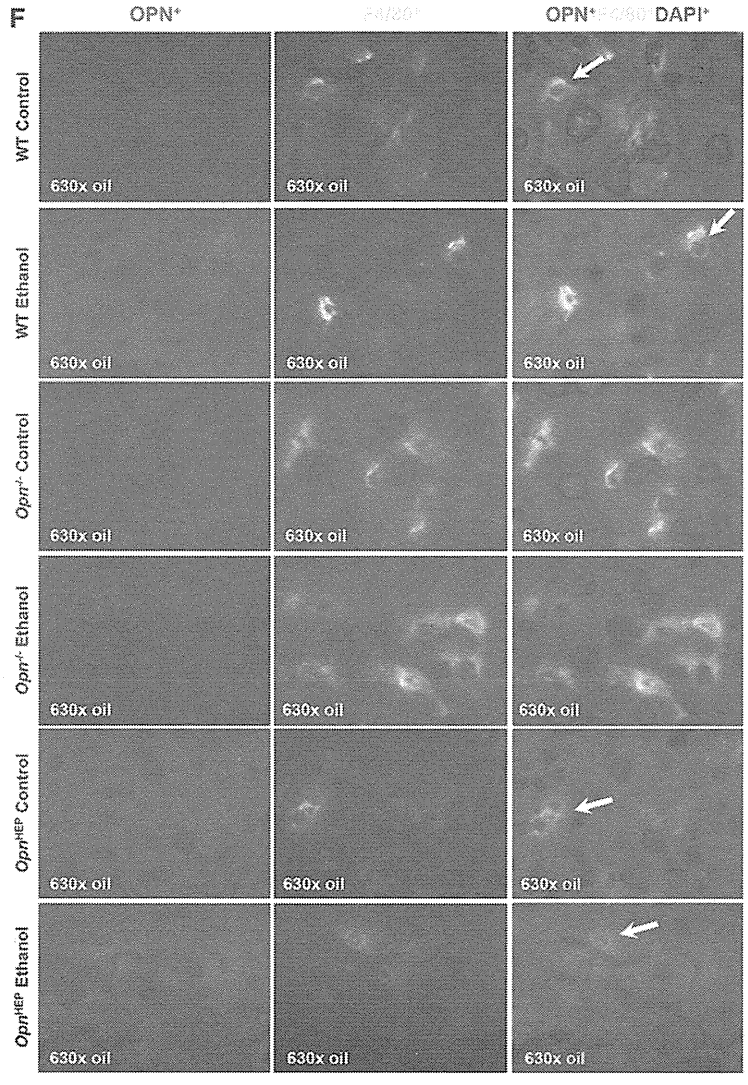

Figure 4 Continuation

76x99mm (300 x 300 DPI)

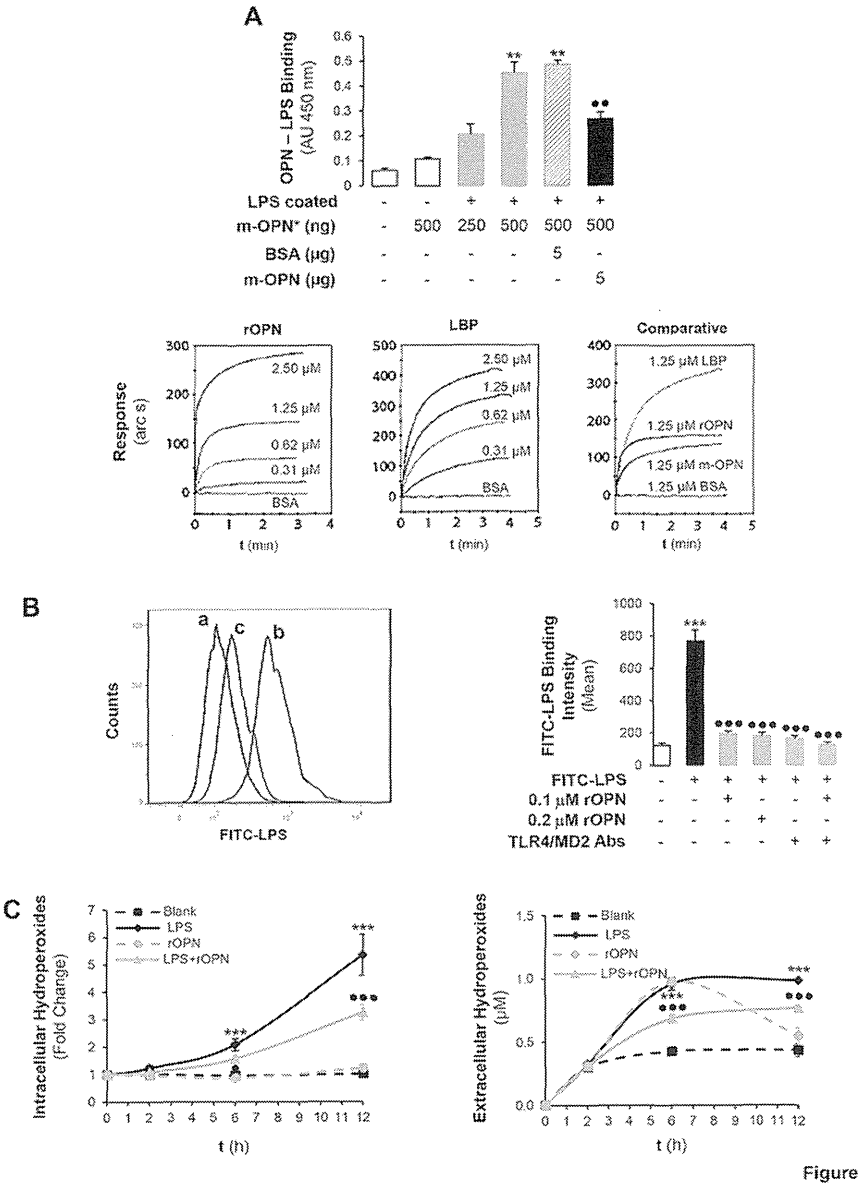

Figure 5

76x98mm (300 x 300 DPI)

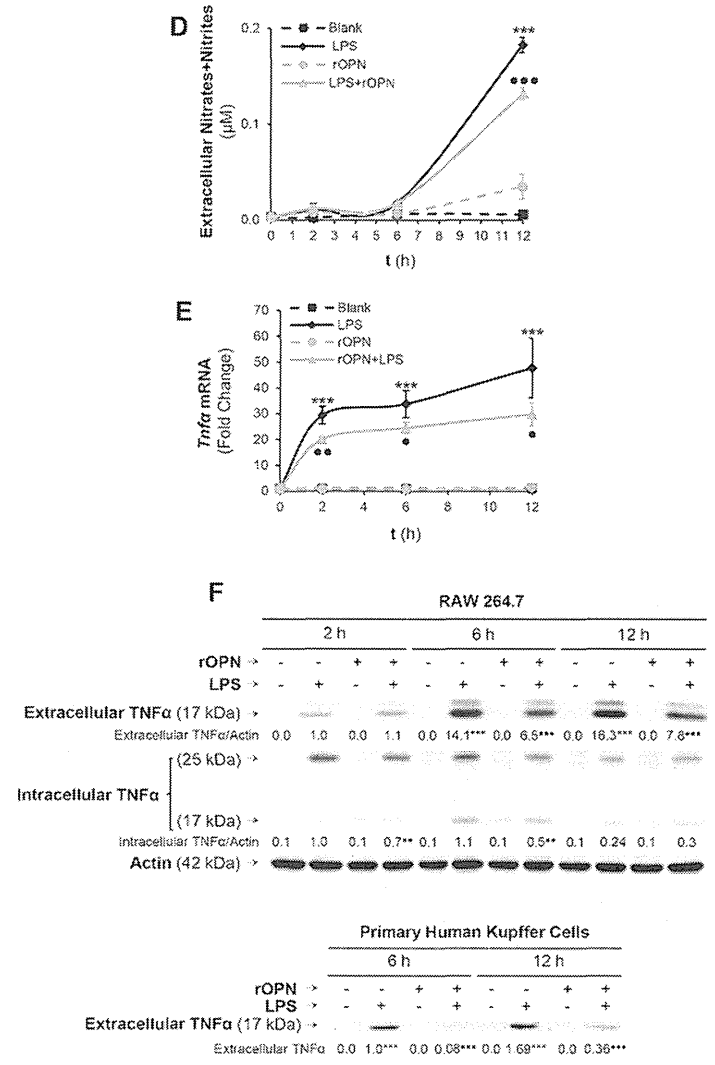

Figure 5 Continuation

76x99mm (300 x 300 DPI)

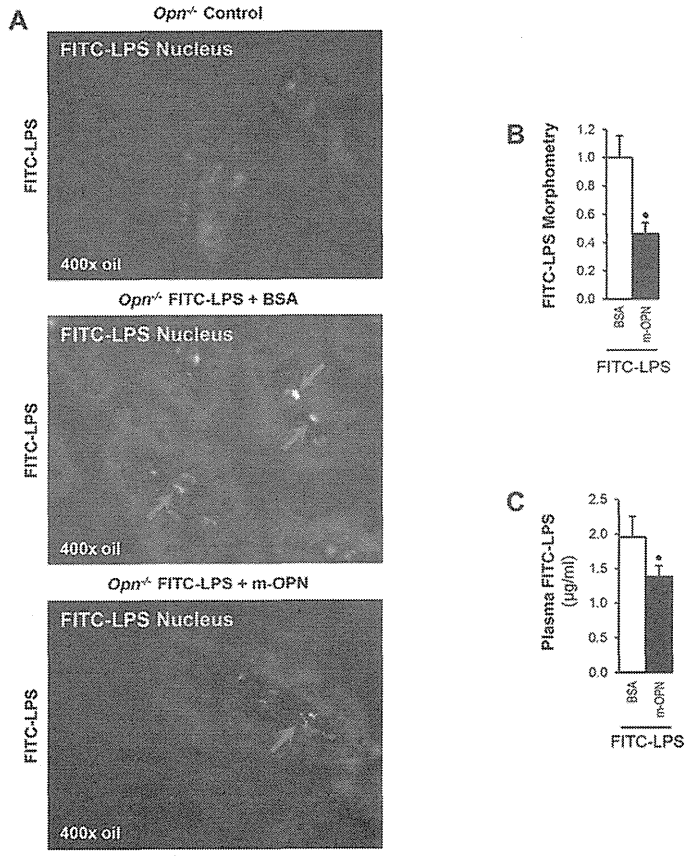

Figure 6

76x99mm (300 x 300 DPI)

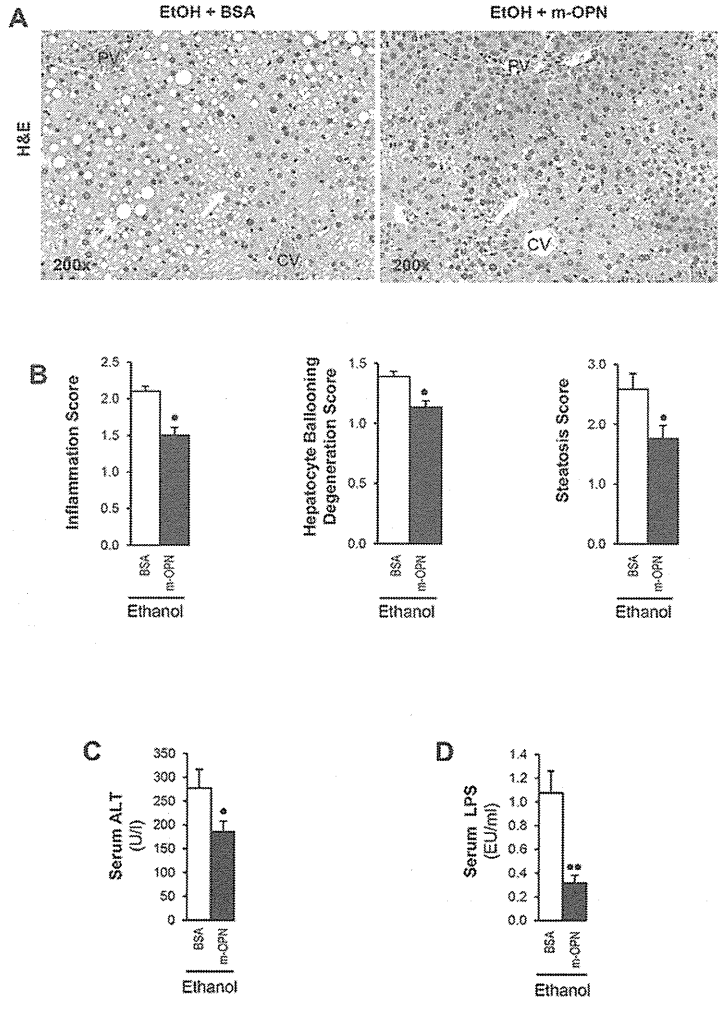

Figure 7

76x99mm (300 x 300 DPI)

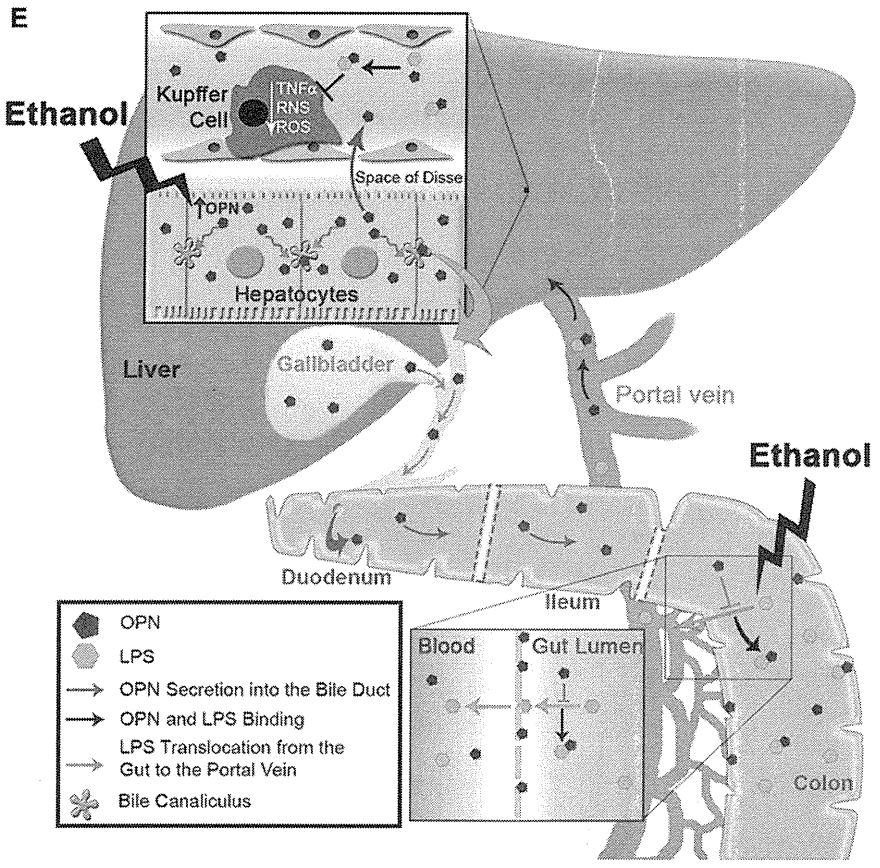

Figure 7 Continuation

76x97mm (300 x 300 DPI)

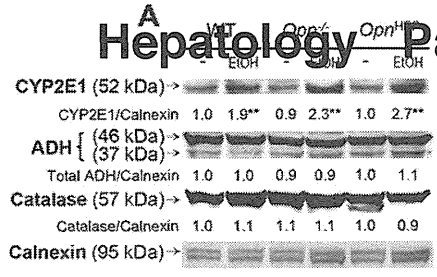

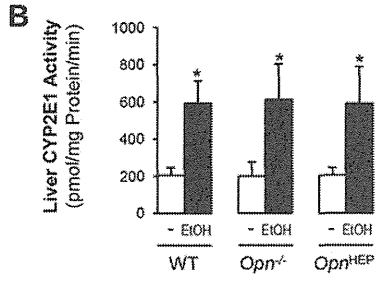

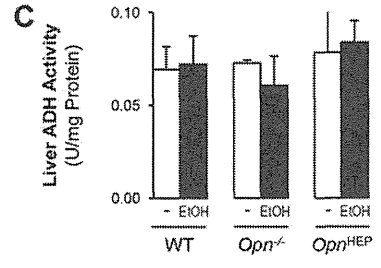

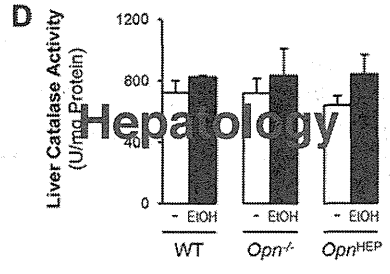

Supplementary Figure 1

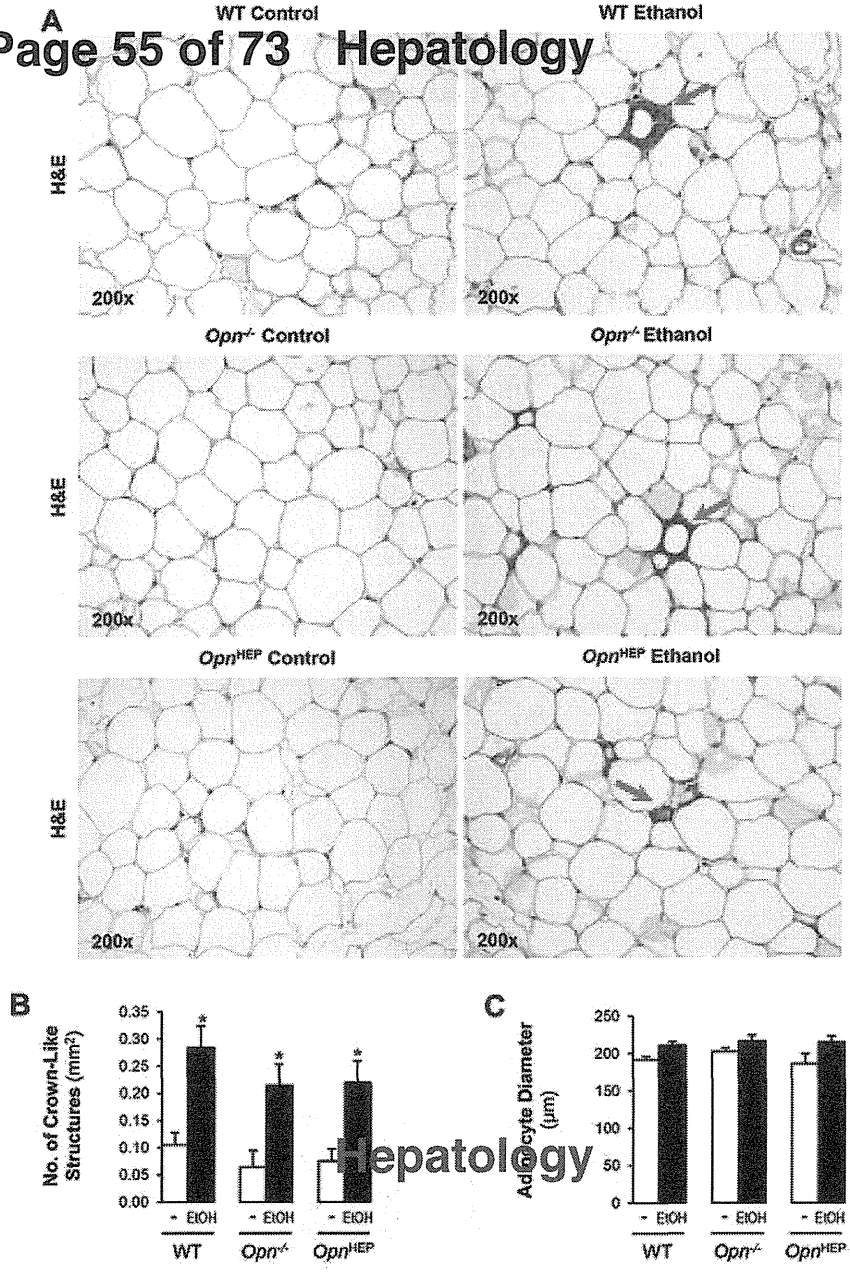

Supplementary Figure 2